

RESEARCH ARTICLE

Emotion Recognition of Partial Face Using Star-Like Particle Polygon Estimation

RATANAK KHOEUN¹, WATCHARAPHONG YOOKWAN¹, PONLAWAT CHOPHUK¹, ANNUPAN RODTOOK², AND KRISANA CHINNASARN¹, (Senior Member, IEEE)

¹Faculty of Informatics, Burapha University, Chonburi 20131, Thailand

²Department of Computer Science, Faculty of Science, Ramkhamhaeng University, Bangkok 10240, Thailand

Corresponding author: Krisana Chinnasarn (krisana@buu.ac.th)

This work was supported by the Faculty of Informatics, Burapha University, Chonburi, Thailand.


ABSTRACT The effectiveness of the existing approaches of facial expression recognition is significantly impacted by the necessity of wearing a facial mask during the Covid-19 outbreak. A large number of significant features on the lower face such as mouth, nose, and cheek, are completely eliminated. In this study, we propose an approach to extract features for recognizing emotions in a partial facial image that is based on Star-Like Particle Polygon Estimation (SLPPE). There are 3 primary steps in the proposed SLPPE. First, the lower part of the original facial input image is obscured by a synthetic mask. The process of representing regions is then used in the upper face image. Secondly, SLPPE is adopted as a feature extraction procedure. It is used to extract probability-based vectors of features that efficiently manifest the occluded facial image's properties. Unlike other CNN based methods that bring the input image known as a raster form into several Conv modules in order to perform feature extraction process, we extract features from the original input image using our proposed SLPPE feature extraction technique in order to eliminate the issues of extracting unexpected features caused by the facial mask region provided by the Conv modules. Our proposed SLPPE feature extraction module produce the potential transformed data in the form of feature vectors without applying Conv modules. Finally, by utilizing LSTM and ANN networks, the SLPPE is adapted to the datasets of CK+, FER2013, and RAF-DB in order to evaluate the proposed methodology. With the accuracy of 99.01%, 98.7%, and 94.62% on CK+, FER2013, and RAF-DB, respectively, our proposed method outperforms the common CNN approaches which are currently in use and yields better results.

INDEX TERMS Emotion recognition, facial expression, feature extraction, feature vectors, occlusion.

I. INTRODUCTION

Applications of emotion recognition in areas such as health-care, security, safe driving, and other areas have helped Facial Emotion Recognition (FER) techniques gain credibility and become widely used in human-computer interaction for intelligent results [1], [2], [3], [4], [5]. When people are going through fundamental emotions, they will show a wide variety of expression patterns on their faces, each with its own personality characteristics and distribution scale [6], [7], [8]. FER is one of the essential elements of human-computer interaction that expand the abilities of computers in recognizing and understanding human

emotions via facial input images. However, in the FER field of study, the existing approaches struggle to deal with scenarios in which wearing a face mask whilst outdoors is advised for everyone. Every application and approach need to handle the same challenge in which mainly the top area of the face is accessible and the lower area is not. FER approaches are divided into different aspects as input type or algorithm type. For the input type aspect, we can also divide FER approaches into two groups; static and dynamics FER approaches. On the other hand, in the algorithm type aspect, there are two distinct categories of approaches; face-based and constituent-based approaches. In the following section, both face-based and constituent-based approaches will be described in either the static or dynamic FER approaches.

The associate editor coordinating the review of this manuscript and approving it for publication was Muhammad Asif .

The advancement of face expression detection technology is essential for the integration of all robots into our daily lives, including autonomous cars and virtual reality. FER was the subject of study using Deep Learning (DL) [9]. On the basis of the created countermeasure network, they proposed a model for occluded expression recognition. In order to supply the face key point angle change feature map with additional information, the AlexNet-Emotion network was proposed. Weber Local Descriptor (WLD)-based emotion recognition that uses occluded facial expressions is proposed in [10]. The occluded facial expressions are reconstructed following an extension approach of Robust Principal Component Analysis (RPCA). The WLD, Histogram of Oriented Gradients (HOG), and Local Binary Patterns (LBP) are the extracted features. KNN and SVM classifiers are used to identify the expressions after the feature vector set has been reduced using Principal Component Analysis (PCA) and Linear Discriminant Analysis (LDA).

A Multi-Feature Fusing Local Directional Ternary Pattern (MFF-LDTP) method for Automatic Facial Expression Signal Recognition (AFESR) at video communication system is presented in [11]. The study adopted Principal Component Analysis (PCA) and enhanced Local Directional Ternary Pattern (LDTP) for AFESR. A research study suggested using quantifiable information on emotions to transform photos with spatiotemporal descriptors into crime prediction images based on a deep convolutional neural network (DCNN) [12]. Another study is about the interaction between audio and visual modalities for cross-modal self-supervision in order to find out if visual self-supervision can improve the learning of speech representation for emotion recognition [13]. However, in order to achieve the result from the method, an extra input source is required which is a high requirement in real-life scenarios. Due to the fact that existing approaches need to use multiple complex structures of the classification process, the idea of extracting essential lightweight features is proposed in order to decrease the complexity and computational time in the classification procedure.

In this paper, we propose a feature extraction technique based on Star-Like Particle Polygon Estimation (SLPPE) that extracts key details about each emotion from images of the upper facial mask. The proposed approach is simple, low complexity, and easy to implement because it can extract a large number of significant features prior to the classification process. Since our lightweight extracted features are translation, scaling, and rotational invariance, a simple structure of classification can be adapted to provide a remarkable result. Proposed Methods, Results and Discussions, and Conclusion were included in the following sections.

II. PROPOSED METHOD

A. EMOTION IN FACIAL IMAGE ANALYSIS

In Facial Emotion Recognition, the number of emotions varies according to the perspective of the various studies. The eight fundamental emotions that we will be focusing on in this paper are Contempt, Anger, Fear, Disgust, Neutral,

Happiness, Sadness, and Surprise. In our research, difficulties arise when every part of the lower face is hidden, making all facial features—including the lips, cheeks, and nose—invisible as shown in Fig. 1. So, the idea is to utilize the existing features of the upper facial image. Moreover, a large number of existing methods are face-based and CNN-based which bring all facial pixels into consideration and a complex structure of classification is required as shown in Fig. 2. Therefore, we came up with an idea of finding the most significant area that can be used to describe a number of different emotions. By doing that, we can utilize a number of regions out of the entire upper facial image and make an essential achievement in recognizing emotions.

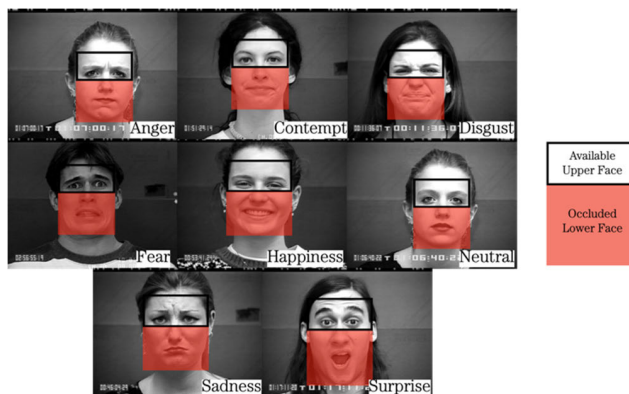


FIGURE 1. Samples of available upper face and occluded lower face input on CK+ dataset.

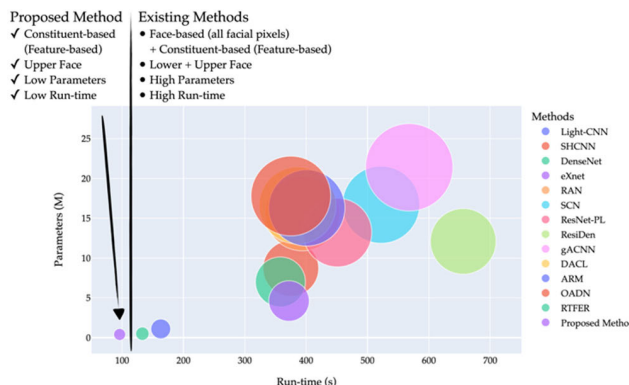


FIGURE 2. Comparison of the common CNN approaches' parameters and run-time on RAF-DB dataset.

From our observation, each emotion affects different parts of the upper face. Every little part sends multi-directional forces to the surrounding area. Each and every force has a variety of directions and magnitudes. As a result, when a particular emotion occurs, multiple regions of the upper face become active. The forces generated by various facial muscles are then represented by a variety of vectors, which also happen in accordance. In addition, each and every emotion has features associated with the area around the eyes and brows, and most crucially, the bridge of the nose, according

to FACs. Therefore, the distance and the pattern between the eyes and eyebrows of the left and right eyes can be used to extract the essential features along with the bridge of the nose for Emotion Recognition.

On the other hand, the Star-Like Particle Polygon Estimation (SLPPE) is used to specify the scope of the area of interest. The features derived from our proposed method are the set of vectors generated from our Probability-based Gradient Vector Flow (PBGVF), where those vectors are only extracted from the ones located inside the proposed SLPPE as shown in Fig. 3. Each vector represents the force between each and every little part of the upper face area. The direction and magnitude of each vector indicate specific information. For the direction perspective, the vector starts from the dark pixel and points to the brighter neighborhood pixel.

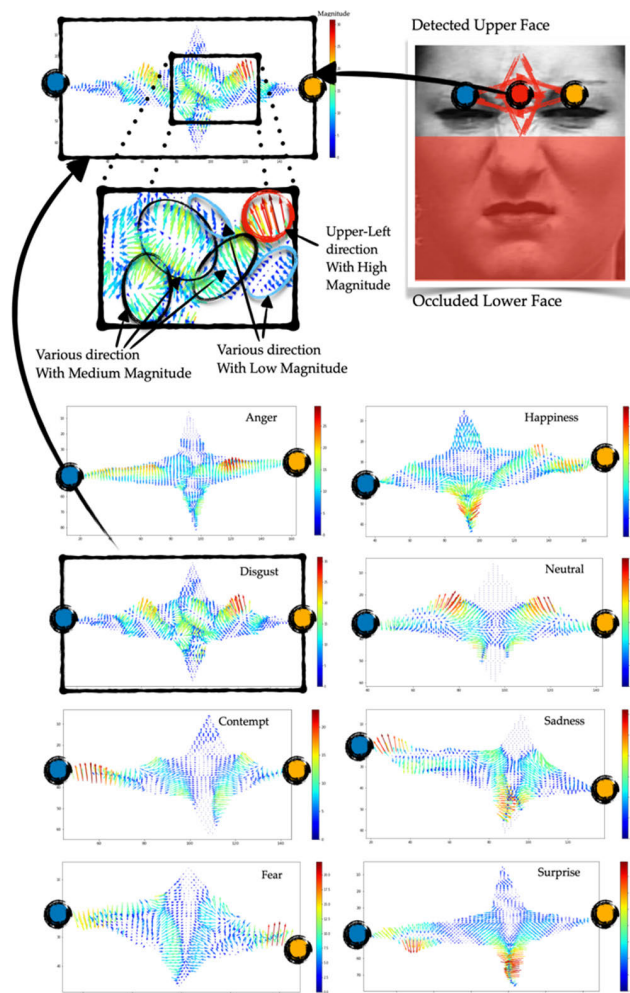


FIGURE 3. Star-Like Particle Polygon of each emotion's sample.

Moreover, the magnitude represents how strong the gradient is between the two neighborhood pixels. So, when the neighbors have an insignificant change of intensity value, the magnitude is apparently low. When the neighboring pixels have highly different intensity values, the magnitude of the vector is remarkably high. From the above-mentioned idea,

the vectors obtained from the flat surface are very low in terms of magnitude while the vectors located at the edges or boundaries of any patterns must have the high remarkable intensity values. The detail of the Star-Like Particle Polygon Estimation (SLPPE) and Probability-Based Modified Gradient Vector Flow (PBGVF) are described in the Proposed Method section.

More importantly, the PBGVF of the dynamic SLPPE is automatically created based on the individual facial upper part. The process of constructing and locating the SLPPE is significantly flexible to the variety of the size between the left and right eyes, eyebrows, and bridge of the nose. It is essential where a number of emotions, and scenarios affect each part of the upper face differently. For instance, Angry, Fear, Disgust, Sad, and Surprise happen to affect the brows and the nose bridge more than other emotions, while Happy affects the upper part of the cheeks. Moreover, flexibility is also very helpful when the size of the left and right eyes and eyebrows are not symmetry. Each and every coordinate of the end of the SLPPE is individually calculated. Moreover, the polygon is able to be rotated in the case where the level of both eyes is not equal.

B. METHODOLOGY

Extracting significant features from the original data, in this case, an occluded facial image, is a critical step for emotion recognition. In this paper, the SLPPE technique is proposed to extract essential features from the upper part of the face. Our proposed method is translation, scaling, and rotation invariant since it is able to automatically specify the location of the centroid of the upper face. We have also discovered that the pattern of each emotion including Anger, Fear, Disgust, Neutral, Happiness, Contempt, Sadness, and Surprise, that happens on the upper face, can be described by the proposed SLPPE technique. The illustration of the proposed method is depicted in Fig. 4. Moreover, the detail of every procedure will be presented in the following sessions.

1) UPPER FACE DETECTION OF A SYNTHETIC MASKED FACE
 In the first step, the facial input image of CK+ dataset [14] is taken into pre-processing step, where the frontal face is detected, apply a synthetic face mask, and then remove the frontal face's lower part. For the face detection process, the Dlib face detector [15] is adopted to detect the face region of the original RGB input image. Then, the lower part including the mouth, nose, and cheeks are covered by a synthetic facial mask to produce a realistic environment. However, the cropped upper parts of frontal faces vary in size.

2) MODIFIED GRADIENT VECTOR FLOW

Several crucial facial features vary depending on the shape, location, size, and direction of their boundaries on each emotion. The Neutral, Happy, and Contempt facial images have similar patterns with the eyes, eyebrows, and bridge of the nose, except with the upper part of the cheeks.

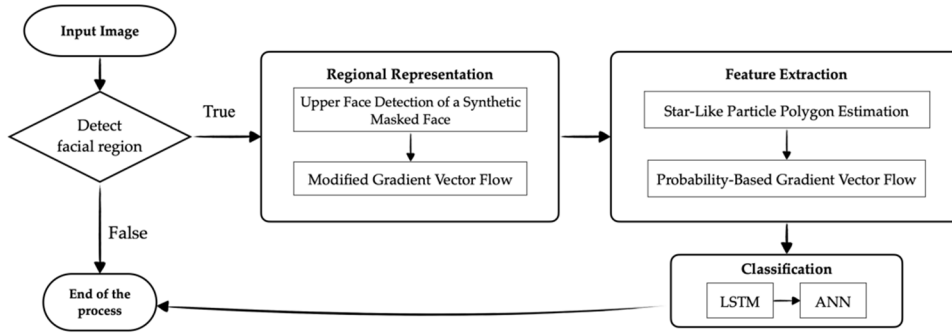


FIGURE 4. The proposed method framework.

For Surprise, the eyebrows are raised up and the eyes happen to be bigger than the other emotions. On the other hand, Angry, Fear, Disgust, and Sadness have a variety of patterns with eyes, eyebrows, and especially with the bridge of the nose. Unlike the original GVF, our Modified GVF has the ability to utilize the forces that happen around the boundary of any region while also decreasing half of the number of vectors which will help to lower the complexity and computational time to the entire process. It is employed to be part of our proposed method in order to convert those significant patterns happening in each emotion into force data that can give us a new point of view in the emotion recognition field.

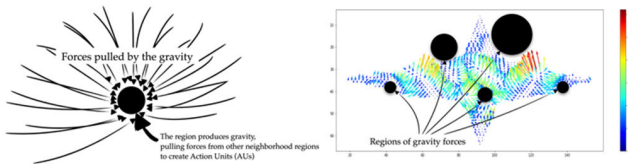


FIGURE 5. Gravity force idea.

The idea is that there are a number of regions that contain gravity, which has the ability to pull neighborhood regions in various directions and magnitudes. This idea corresponds to the corresponds to Action Units (AUs) which are triggered by any emotions on the upper face. Due to the fact that there could be multiple regions with gravity forces, it would produce multiple vectors with different directions and magnitudes as shown in Fig. 5.

The vector field $v(x, y) = (u(x, y), v(x, y))$ called the gradient vector flow (GVF) field reduces the energy function as in Equation (1).

$$\varepsilon = \iint \mu (u_x^2 + u_y^2 + v_x^2 + v_y^2) + |\nabla f|^2 |v - \nabla f|^2 dx dy \tag{1}$$

The formulation corresponds to the conventional concept of smoothing the outcome in the absence of data. Particularly, we discover that the vector field's partial derivatives dominate the energy when $|df|$ is small, producing a smooth field. When the $|df|$ is large, on the other hand, the integrand is dominated by the second term, which is reduced by $v = df$. The trade-off among the initial and secondary terms is

determined by the regularization parameter m . The parameter needs to be set in accordance with the level of noise in the image.

$$\mu \nabla^2 u - (u - f_x) (f_x^2 + f_y^2) = 0 \tag{2}$$

$$\mu \nabla^2 v - (v - f_x) (f_x^2 + f_y^2) = 0 \tag{3}$$

where dS is the Laplacian operator. An additional comprehension of the MGVF formulation is provided by Equations (2) and (3). Since the gradient of $f(x, y)$ is zero in homogeneous regions, the second terms of both equations are zero. As a result, Laplace's equation can be employed to determine both u and v within these regions. This resulted in some information being filled in from the region's boundaries.

By calculating the MGVF field of the upper frontal face, we then achieve a set of vectors indicating the forces in all regions. Each force vector varies in direction and magnitude. The magnitude of the vectors is high at the edge or boundary of regions, and low on a smooth surface. Moreover, the direction of the vectors starts from the low-intensity region and ends up at the higher-intensity region compared to the starting point. With the variety of the direction and magnitude of vectors in the GVF field, the essential information on the upper face produced by each emotion is utilized.

3) STAR-LIKE PARTICLE POLYGON ESTIMATION

Following that the MGVF field is calculated throughout the entire upper part of the face, instead of bringing all series of vectors straight to the classification process, we extract only a crucial set of vectors from the entire MGVF field. The amount of computational time is significantly reduced by lowering the number of vectors.

For the purpose of defining a crucial set of vectors, there are three main challenges involved. The first challenge is to discover the relevant location for the SLPPE. It corresponds to the idea that the pattern of the region located at the bridge of the nose is prioritized. Therefore, locating the SLPPE in the most relevant position is a must before moving to the next step. The second challenge is to make each end of the SLPPE independently scalable. This is a flexible solution for the scenarios in that the size of the left and right eyes is distinctive. The third challenge is to rotate the polygon either

clockwise or counterclockwise with the relevant amount of angle. So, our proposed method is significantly flexible for various scenarios of the frontal face in terms of translation, scale, and rotational invariance.

With regard to the first challenge, our proposed dynamic SLPPE needs to be located in the correct position. To be more precise, the SLPPE needs to be placed where its centroid matches the bridge of the nose, which is considered the center between the left and right eye regions. Since the bridge of the nose is not always the center of the upper part image, we need to find the unique MGVF field relationship that happens at the center of the bridge compared to the other area. Due to the fact that the magnitude of MGVF vectors is large at the boundary or edge of regions while there are more edges on either the eyes and eyebrows than on the bridge of the nose, the magnitude of MGVF vectors at the bridge of the nose is significantly lower compared to the eye regions as shown in Fig. 6.

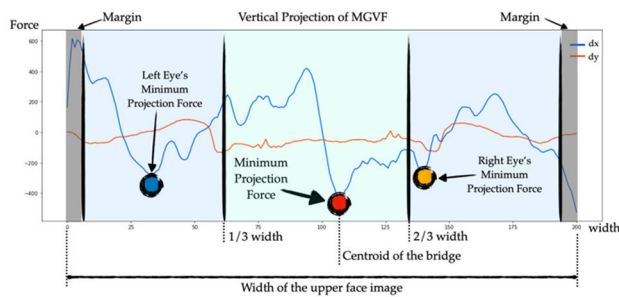


FIGURE 6. Star-like particle polygon translation and scaling.

Relating to the second challenge, once the polygon is placed in the correct position, another challenge is to dynamically calculate and define the size of the polygon. Due to the fact that the eyes and eyebrows regions differ in size between the left and the right, the size of each end of the SLPPE needs to be dynamically calculated. Starting with the coordinate of the new centroid, the upper face is divided into 2 parts. The horizontal projection of the Modified GVF in the Y-coordinate is then calculated independently. The coordinates in which the horizontal projection of MGVF has the highest value are then considered the coordinate of the left and right ends of the SLPPE. On the other hand, the height of the polygon equals to the height of the upper face image without the margin m . By doing this, the polygon can be individually scaled according to the size of each eye as shown in Fig. 6.

More importantly, the left and right eyes also vary in the horizontal level, meaning one of both eyes and eyebrows is higher than the other. Therefore, having only the correct location and size is not enough. The SLPPE also needs to be rotatable either clockwise or counterclockwise according to the horizontal level of both eyes. The polygon should be rotated clockwise when the eye and eyebrows on the left of the facial image are higher than the ones on the right, and vice versa.

In order to compare the horizontal level between both eyes, the horizontal projection of the GVF is performed. In consideration of the fact that the proposed MGVF vectors start pointing from the darker to the brighter area, the upper boundary of the eyebrows will have the MGVF vectors pointing upwards to the forehead. On the other hand, the lower boundary of the eyebrows will have the MGVF pointing downwards to the eyes. Therefore, the gradient value of each vector on the Y-coordinate along the eyebrows' area, is most likely to be larger compared to the one on the X-coordinate.

The horizontal projection of the MGVF needs to be achieved separately between both sides. Starting with the established centroid, the image is divided into 2 parts according to the centroid's X-coordinate. The horizontal projection of each region is then calculated individually. As shown in Fig. 7, the peak of each graph indicates the location where the total horizontal amount of MGVF on the Y-coordinate has reached the highest value. In the case that the peaks of both eyes have the same horizontal level, the proposed SLPPE will not be rotated. On the other hand, if the peak of one side is higher than the other, then the polygon will be rotated toward the lower side.

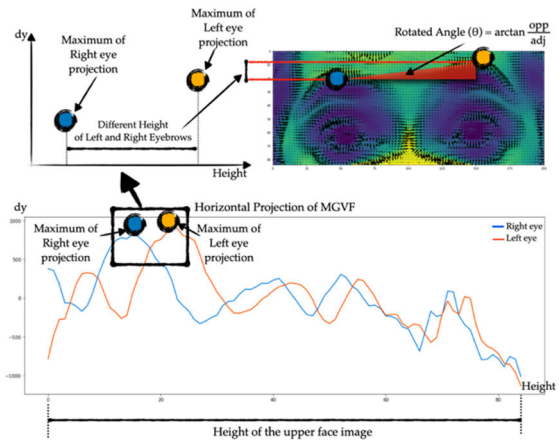


FIGURE 7. Star-like particle polygon rotation.

Furthermore, the next process is to calculate the amount of angle that the polygon will be rotated. By finding the different distances between the height of the peaks, we then achieve the opposite side of θ . Moreover, the distance between the peaks in X-coordinate is the adjacent side of the θ . The amount of angle that the polygon needs to be rotated is $\theta = \arctan(opp/adj)$. By completing the process, the polygon can be independently rotated according to the environment of the upper face.

4) PROBABILITY-BASED GRADIENT VECTOR FLOW

In this section, the PBGVF is described in a probabilistic perspective. The SLPPE is the combination of a number of regions as shown in Fig. 8. The idea is that, when the proposed star-shape polygon is overlapped with the upper face at the correct location, size and angle, a set of SLPPE inside

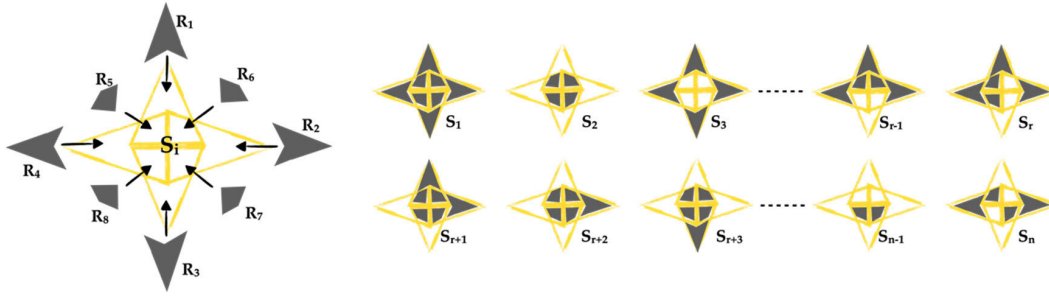


FIGURE 8. Star-like particle polygon.

the polygon is activated. With the same emotion, the same number and location of regions should be activated inside the polygon and vice versa. However, our purpose of this process is to specify the activated regions inside the SLPPE for each individual emotion including Anger, Fear, Disgust, Neutral, Contempt, Happiness, Sadness, and Surprise. Let's say we have $P(S_1)$ as the probability of a star-like polygon with all of its regions being activated. $P(S_2)$ is the probability of the polygon where only the middle parts are activated. $P(S_3)$ is the probability of another polygon where only the 4 edge triangles are activated, and so on. By the end of the variety of the activated regions, we have $P(S_n)$ where n is the number of possible combinations. The probability of each Emotion given the number of different activated shapes; S_1, S_2, \dots, S_n , inside the polygon in different emotions, is shown in Equation (4).

$$P(Emotion|S_i) = \frac{P(S_i|Emotion)P(Emotion)}{P(S_i)} \quad (4)$$

where $i = \{1, 2, \dots, n\}$, S_i is the star-like polygon with different activated areas, and $P(S_i) = \sum_{j=0}^8 P(R_j)$. Moreover, $P(R_j)$ is the probability of each small activated region inside S_i as depicted in Fig. 8.

We adopt Expectation Maximization (EM) in order to specify the activated shapes for each emotion. Only a number of shapes that makes each emotion obtains the highest value of the probability $P(Emotion|S_1, S_2, \dots, S_n)$ is selected as in Equation (5).

$$\hat{\theta} = \operatorname{argmax}_{\theta} \log(\sum_S P(Emotion, S|\theta)) \quad (5)$$

where $\hat{\theta}$ is the goal of the Expectation Maximization (EM), $Emotion$ is a set of the observed data, and S is a set of unobserved latent data.

More importantly, the idea is to calculate and construct a transforming matrix A that has the ability to transform the original detected set of PBGVF to match the expected result. The probability result of each emotion is then considered as the target label matrix Y of each emotion. Therefore, the transforming matrix of the PBGVF X is $A = X^{-1}Y$, where X^{-1} is the inverse of X .

5) CLASSIFICATION

The proposed extracted features using SLPPE are taken as the input to the classification process. In order to classify the

TABLE 1. Results of existing approaches on FER2013.

Approaches	Accuracy (%)	Parameters (M)
Simple-CNN [18]	59.18	0.6
PyFER [19]	60.16	3.9
MobileNet [20]	61.13	3.2
Inception v.1 [21]	61.12	6.4
ResNet 50 [22]	64.22	25.6
Xception [23]	63.99	0.2
Proposed Method	98.7	0.3

TABLE 2. Results of existing approaches on CK+.

Approaches	Accuracy (%)	Parameters (M)
Light-CNN [24]	92.86	1.1
eXnet [25]	95.81	4.6
Pre-trained CNN [24]	95.29	7.1
PG-CNN [26]	97.03	20.5
DLP-CNN [17]	95.73	17.5
gACNN [27]	96.40	21.4
RASnet [28]	96.28	10.4
DeRL [29]	97.30	21.1
RTFER [28]	93.85	0.5
Proposed Method	99.01	0.3

TABLE 3. Results of existing approaches on RAF-DB.

Approaches	Accuracy (%)	Parameters (M)
ResiDen [30]	76.54	12.1
Light-CNN [24]	77.23	1.1
SHCNN [31]	81.17	8.7
DenseNet [32]	81.93	7
gACNN [27]	85.07	21.4
eXnet [25]	85.59	4.6
ResNet-PL [33]	86.97	13.2
RAN [34]	86.99	15.6
SCN [35]	87.03	16.7
OADN [36]	87.16	17.8
DAFL [37]	87.78	16.6
Proposed Method	94.62	0.3

input data, LSTM and ANN are adopted with as shown in Fig. 9. Unlike other CNN based methods that bring the input image known as a raster form into several Conv modules in order to perform feature extraction process, we firstly extract

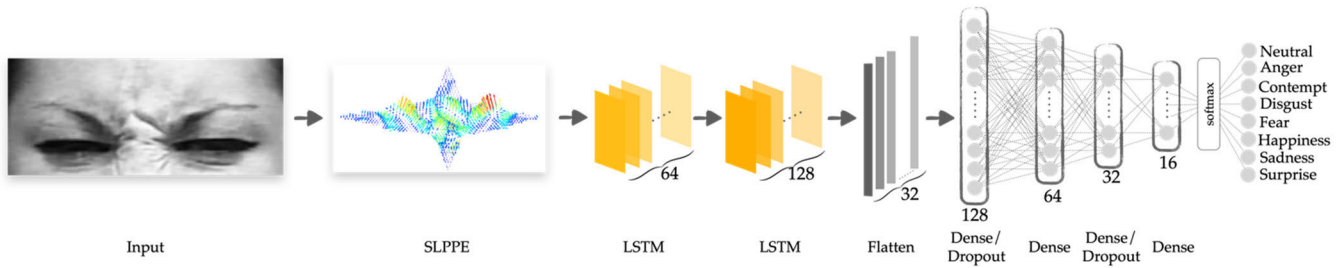


FIGURE 9. Classification structure.

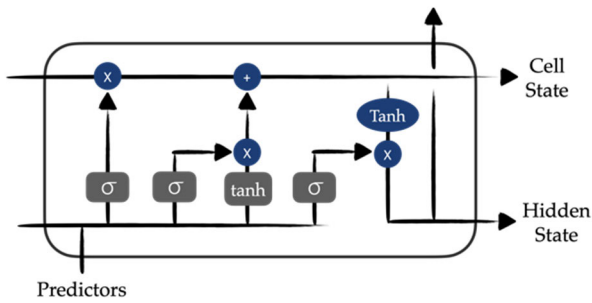


FIGURE 10. LSTM structure.

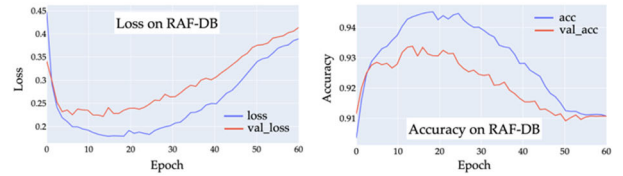
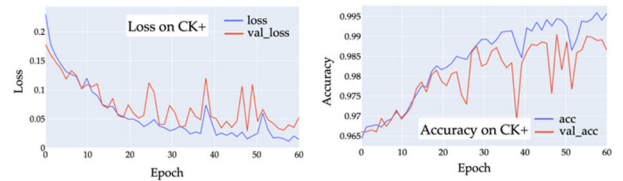
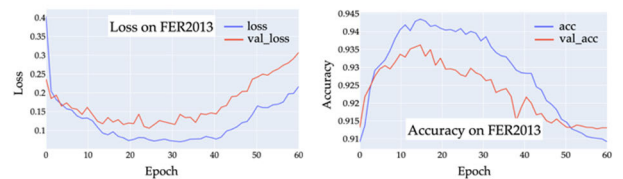
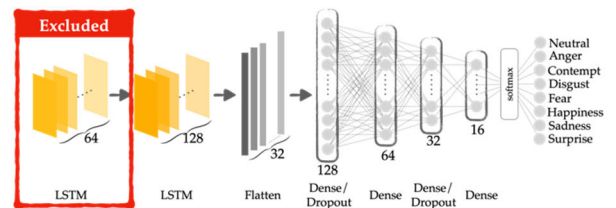


FIGURE 12. Results of FER2013, CK+, and RAF-DB dataset without LSTM (64) module.

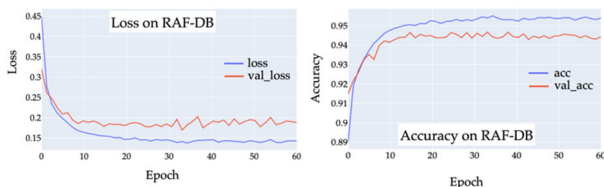
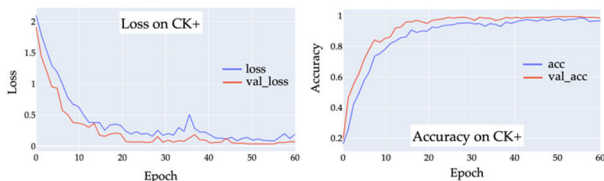
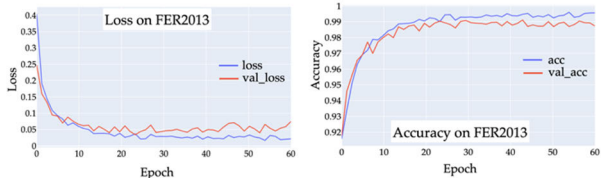
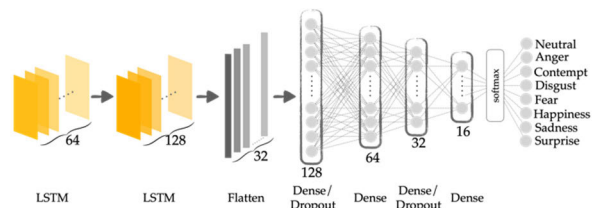


FIGURE 11. Results of FER2013, CK+, and RAF-DB dataset with all proposed modules.

features from the original input image using our proposed feature extraction technique. In order to eliminate the issues of extracting unexpected features caused by the facial mask region provided by the Conv modules, our proposed SLPPE

feature extraction module produce the potential transformed data in the form of feature vectors without applying Conv modules. Those feature vectors that are the representative of each emotion, are brought into the LSTM modules. Two LSTM layers are used before adapting Flatten layer and pushing to a number of Dense layers. Additionally, the Dropout Layer is applied after the first and third Dense layers in order to avoid over fitting. Moreover, the Softmax activation function is used at the final Dense layer of classification. Eventually, the network is trained with the loss function of the categorical cross entropy along with the Adam optimizer and the learning rate of 0.001.

The neural networks in Fig. 10 reflect the LSTM components' gates and display the data gathered from the predictors and the preceding cell. The function of tanh that modify the nodes' weights get the data from these gates. This results in

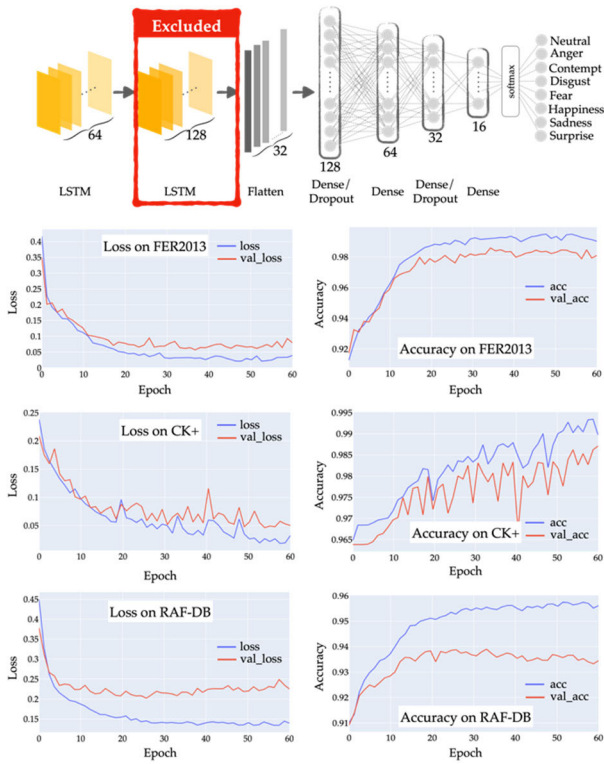


FIGURE 13. Results of FER2013, CK+, and RAF-DB dataset without LSTM (128) module.

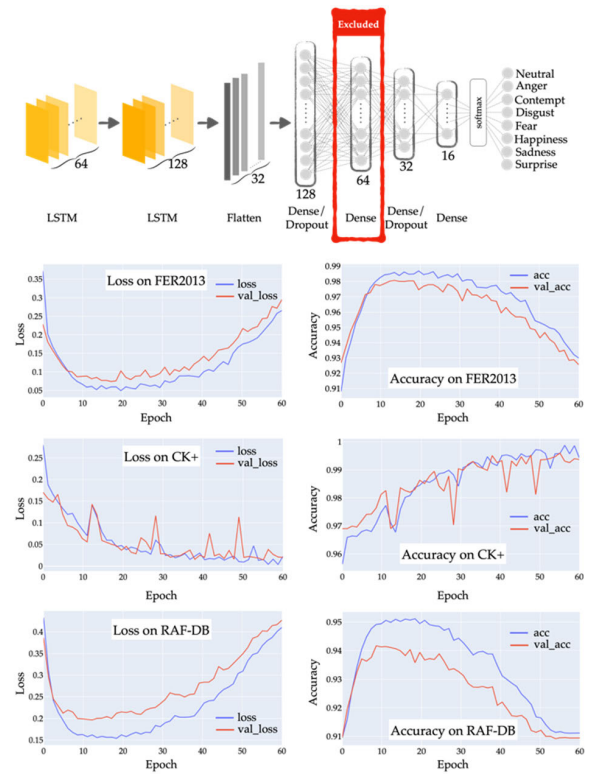


FIGURE 15. Results of FER2013, CK+, and RAF-DB dataset without Dense (64) module.

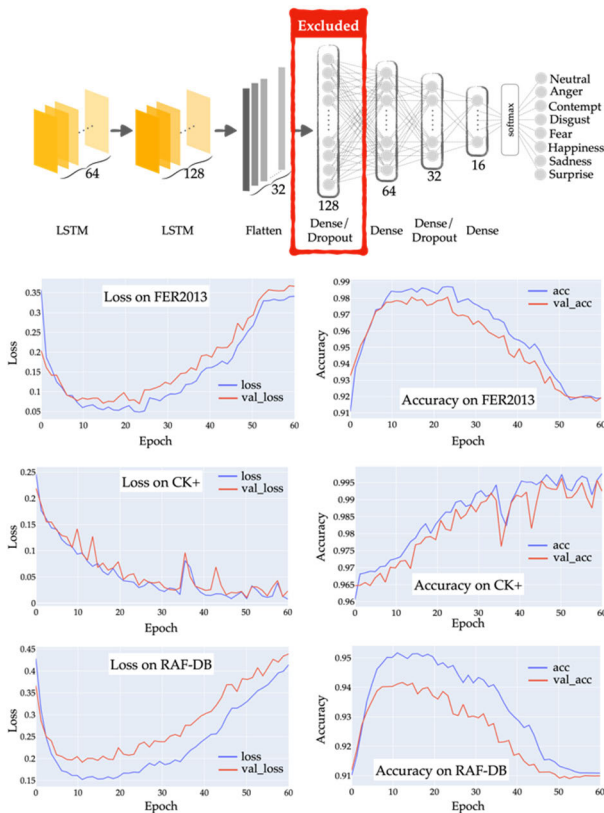


FIGURE 14. Results of FER2013, CK+, and RAF-DB dataset without Dense/Dropout (128) module.

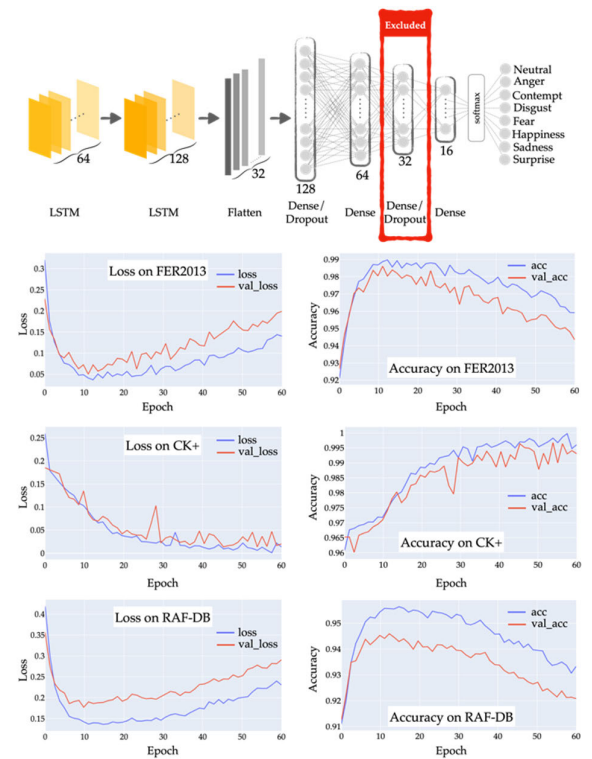


FIGURE 16. Results of FER2013, CK+, and RAF-DB dataset without Dense/Dropout (32) module.

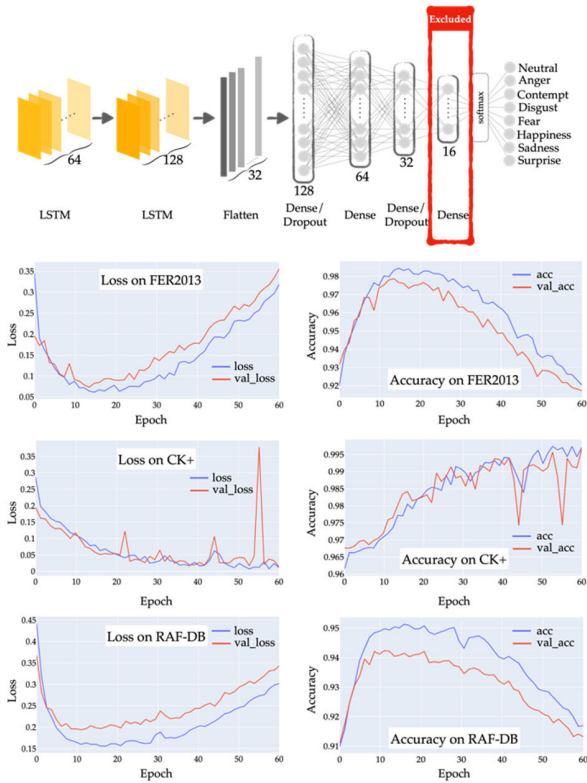


FIGURE 17. Results of FER2013, CK+, and RAF-DB dataset without Dense (16) module.

the formation of both short-term (hidden state) and long-term (cell state) memory. The amount of long-term knowledge that should be lost is determined by the forget gate. A cell’s state is determined by the information that is retained. Furthermore, it establishes the amount of recent data that the input gate should disregard. The tanh functions are then given the data to train on. The output gate, last but not least, decides how much data to transmit into the concealed state based on Equation (6) using the two types of short and long-term memory.

$$c_t = f_t \odot c_{t-1} + i_t \odot \tilde{c}_t \tag{6}$$

where c_{t-1} is the prior cell state, f_t is the forget gate, i_t is the input gate, and \tilde{c}_t is the intermediary cell state.

$$f_t = \left(\frac{t - k_t + 1}{t - k_t} \right)^{-p} \tag{7}$$

where t is the current time step’s index, p regulates the rate of information decay, and the earliest timestamp of interest’s index is k_t . Moreover, the forget gate in Equation (7) specifies the time range for searching in long-term memory.

$$k_t = r_t \odot t + (1 - r_t) \odot k_{t-1} \tag{8}$$

The reset gate, r_t , is a sigmoid activation function, as indicated in Equation (8). This particularly implies that the gate receives a value in the range of 0 and 1. In the case that its value is 1, k_{t-1} is terminated, and all prior information is removed. On the other hand, in the case that the value is 0, t is terminated, however, the previous information is maintained.

III. RESULTS AND DISCUSSIONS

We used the FER2013 [16], CK+ [14], and RAF-DB [17] datasets in the research we performed. As demonstrated in Fig. 11, using data obtained from both datasets, the curve of learning for accuracy and loss throughout the training and validation shows that the learning outcomes are in the optimal fitting context and that the losses of training and validation converge at a level where the gap between both of the final loss values is negligible. The study was conducted in a subject-independent manner, where the training and testing set of data were split up from each other. The training and testing set was set to be 75% and 25% of each dataset, respectively. Our proposed SLPPE module provides effective information of detected features to the classification process. As shown in Tables 1, 2 and 3, we achieve 99.01%, 98.7%, and 94.62% accuracy for the datasets from CK+, FER2013, and RAF-DB, respectively.

Moreover, due to the fact that each dataset has different size, head posture, and occlusion (such as glasses, facial hair, or self-occlusion) of the input images, they are unapplicable for some methods. Thus, a number of different methods were compared for different datasets as shown in Tables 1, 2 and 3. More importantly, those methods were performed using CNN based feature extraction technique where a number of Conv modules were adopted.

In our work, the dataset from CK+ is utilized. It includes 123 subjects’ 593 acted facial expression sequences representing 8 baseline emotions including Anger, Fear, Disgust, Neutral, Happiness, Contempt, Sadness, and Surprise. Neutral baseline and apex ending point are present in the expression image sequences. More importantly, among each and every facial expression image sequence, it starts with the Neutral at the very first frame and ends with a certain expression considered as the apex image at the very last frame of the sequence. Our research, however, focuses on recognizing emotion from a single image; particularly, our method only uses the participant’s apex image which is the last frame of each image sequence as our input image. Additionally, some of the subjects demonstrated multiple emotions, therefore more than one image was obtained from those participants.

Moreover, FER2013 is also used in our experiment. The images of FER2013 were created using the Google image search API. It is referred to be a large-scale, unrestricted database that presents crucial difficulties for ongoing studies. In order to create bounding boxes around each face in the gathered photos, OpenCV face recognition was employed. Then, FER2013’s human labeler team rejected photographs with inaccurate labels, fixed some cropping issues, and eliminated some duplicate images. After improperly identified frames were removed and the cropped area was modified, the FER2013 dataset provides us with the images that were already registered and downsized to 48*48 pixels. FER2013 comprises 28,709 training images, 3,589 validation images, and 3,589 testing images with seven expression labels. The dataset contains 7 baseline emotions including Angry, Disgust, Fear, Happy, Sad, Surprise, and Neutral. On the other

TABLE 4. Results of the proposed method on each emotion with all proposed modules.

Emotions	FER2013				CK+				RAF-DB			
	Precis.	Recall	F1	Acc.	Precis.	Recall	F1	Acc.	Precis.	Recall	F1	Acc
Neutral	0.989	0.999	0.994	0.999	1.00	1.00	1.00	1.00	0.980	0.984	0.983	0.984
Anger	0.933	0.792	0.857	0.792	1.00	0.933	0.965	0.933	0.746	0.644	0.691	0.644
Disgust	0.839	0.812	0.825	0.812	1.00	1.00	1.00	1.00	0.739	0.310	0.437	0.310
Fear	0.971	0.862	0.913	0.862	1.00	1.00	1.00	1.00	0.493	0.746	0.594	0.746
Happy	0.979	0.848	0.909	0.848	1.00	1.00	1.00	1.00	0.182	0.008	0.015	0.008
Sadness	0.953	0.875	0.912	0.875	1.00	0.916	0.956	0.916	0.00	0.00	0.00	0.00
Surprise	0.970	0.899	0.933	0.899	1.00	1.00	1.00	1.00	0.821	0.887	0.853	0.887
Contempt	-	-	-	-	0.667	1.00	0.80	1.00	-	-	-	-

TABLE 5. Results of the proposed method on each emotion without LSTM (64) module.

Emotions	FER2013				CK+				RAF-DB			
	Precis.	Recall	F1	Acc.	Precis.	Recall	F1	Acc.	Precis.	Recall	F1	Acc
Neutral	0.921	0.998	0.958	0.998	0.993	0.999	0.996	0.999	0.910	0.999	0.983	0.999
Anger	0.50	0.011	0.021	0.011	0.850	0.919	0.883	0.919	0.00	0.00	0.00	0.00
Disgust	0.00	0.00	0.00	0.00	1.00	0.461	0.632	0.461	0.00	0.00	0.00	0.00
Fear	0.00	0.00	0.00	0.00	0.925	0.960	0.942	0.960	0.00	0.00	0.00	0.00
Happy	0.370	0.021	0.0394	0.021	0.895	0.629	0.739	0.629	0.00	0.00	0.00	0.00
Sadness	0.125	0.003	0.0059	0.003	0.847	0.813	0.829	0.813	0.00	0.00	0.00	0.00
Surprise	0.00	0.00	0.00	0.00	0.720	0.643	0.679	0.643	0.00	0.00	0.00	0.00
Contempt	-	-	-	-	0.879	0.542	0.670	0.542	-	-	-	-

TABLE 6. Results of the proposed method on each emotion without LSTM (128) module.

Emotions	FER2013				CK+				RAF-DB			
	Precis.	Recall	F1	Acc.	Precis.	Recall	F1	Acc.	Precis.	Recall	F1	Acc
Neutral	0.986	0.994	0.990	0.994	0.995	0.996	0.996	0.996	0.960	0.988	0.974	0.988
Anger	0.876	0.808	0.841	0.808	0.939	0.911	0.925	0.911	0.00	0.00	0.00	0.00
Disgust	0.833	0.483	0.612	0.483	0.625	0.714	0.666	0.714	0.111	0.044	0.063	0.044
Fear	0.862	0.795	0.827	0.795	0.910	1.00	0.953	1.00	0.448	0.448	0.448	0.448
Happy	0.904	0.821	0.860	0.821	1.00	0.571	0.727	0.571	0.139	0.035	0.056	0.035
Sadness	0.846	0.744	0.791	0.744	0.808	0.737	0.771	0.737	0.00	0.00	0.00	0.00
Surprise	0.837	0.787	0.811	0.787	0.333	0.241	0.280	0.241	0.769	0.661	0.711	0.661
Contempt	-	-	-	-	0.687	0.782	0.731	0.782	-	-	-	-

TABLE 7. Results of the proposed method on each emotion without Dense/Dropout (128) module.

Emotions	FER2013				CK+				RAF-DB			
	Precis.	Recall	F1	Acc.	Precis.	Recall	F1	Acc.	Precis.	Recall	F1	Acc
Neutral	0.919	0.999	0.957	0.999	0.999	0.999	0.999	0.999	0.910	0.999	0.952	0.999
Anger	0.00	0.00	0.00	0.00	0.902	1.00	0.948	1.00	0.00	0.00	0.00	0.00
Disgust	0.00	0.00	0.00	0.00	0.727	1.00	0.842	1.00	0.00	0.00	0.00	0.00
Fear	0.00	0.00	0.00	0.00	0.893	0.967	0.929	0.967	0.00	0.00	0.00	0.00
Happy	0.440	0.046	0.083	0.046	1.00	0.714	0.833	0.714	0.00	0.00	0.00	0.00
Sadness	0.00	0.00	0.00	0.00	0.905	0.955	0.929	0.955	0.00	0.00	0.00	0.00
Surprise	0.00	0.00	0.00	0.00	0.833	0.689	0.754	0.689	0.00	0.00	0.00	0.00
Contempt	-	-	-	-	0.941	0.897	0.918	0.897	-	-	-	-

TABLE 8. Results of the proposed method on each emotion without Dense (64) module.

Emotions	FER2013				CK+				RAF-DB			
	Precis.	Recall	F1	Acc.	Precis.	Recall	F1	Acc.	Precis.	Recall	F1	Acc
Neutral	0.924	0.998	0.959	0.998	0.995	0.999	0.997	0.999	0.909	1.00	0.952	1.00
Anger	0.428	0.058	0.103	0.058	1.00	0.842	0.914	0.842	0.00	0.00	0.00	0.00
Disgust	0.00	0.00	0.00	0.00	0.857	1.00	0.923	1.00	0.00	0.00	0.00	0.00
Fear	0.548	0.057	0.104	0.057	1.00	1.00	1.00	1.00	0.00	0.00	0.00	0.00
Happy	0.864	0.101	0.181	0.101	0.941	0.941	0.941	0.941	0.00	0.00	0.00	0.00
Sadness	0.50	0.003	0.006	0.003	0.890	0.780	0.832	0.780	0.00	0.00	0.00	0.00
Surprise	0.636	0.064	0.116	0.064	0.666	0.640	0.653	0.640	0.00	0.00	0.00	0.00
Contempt	-	-	-	-	0.953	0.670	0.787	0.670	-	-	-	-

TABLE 9. Results of the proposed method on each emotion without Dense/Dropout (32) module.

Emotions	FER2013				CK+				RAF-DB			
	Precis.	Recall	F1	Acc.	Precis.	Recall	F1	Acc.	Precis.	Recall	F1	Acc
Neutral	0.937	0.992	0.964	0.992	0.997	0.998	0.998	0.998	0.9192	0.995	0.955	0.995
Anger	0.599	0.460	0.520	0.460	1.00	0.909	0.954	0.909	0.60	0.034	0.064	0.034
Disgust	0.625	0.185	0.285	0.185	0.909	0.769	0.833	0.769	0.272	0.012	0.023	0.012
Fear	0.788	0.137	0.234	0.137	0.936	1.00	0.967	1.00	0.381	0.081	0.134	0.081
Happy	0.707	0.186	0.295	0.186	0.863	0.904	0.883	0.904	0.00	0.00	0.00	0.00
Sadness	0.632	0.220	0.327	0.220	0.936	0.977	0.956	0.977	0.00	0.00	0.00	0.00
Surprise	0.550	0.244	0.339	0.244	0.952	0.833	0.888	0.833	0.556	0.164	0.253	0.164
Contempt	-	-	-	-	0.895	0.796	0.843	0.796	-	-	-	-

TABLE 10. Results of the proposed method on each emotion without Dense (16) module.

Emotions	FER2013				CK+				RAF-DB			
	Precis.	Recall	F1	Acc.	Precis.	Recall	F1	Acc.	Precis.	Recall	F1	Acc
Neutral	0.917	0.998	0.956	0.998	0.997	0.997	0.998	0.997	0.910	0.999	0.953	0.999
Anger	0.00	0.00	0.00	0.00	1.00	0.694	0.819	0.694	0.00	0.00	0.00	0.00
Disgust	0.00	0.00	0.00	0.00	0.50	1.00	0.666	1.00	0.00	0.00	0.00	0.00
Fear	0.00	0.00	0.00	0.00	0.923	0.967	0.944	0.967	0.00	0.00	0.00	0.00
Happy	0.666	0.024	0.047	0.024	1.00	0.636	0.777	0.636	0.00	0.00	0.00	0.00
Sadness	0.666	0.005	0.011	0.005	0.898	0.898	0.898	0.898	0.00	0.00	0.00	0.00
Surprise	0.189	0.031	0.053	0.031	0.952	0.80	0.869	0.80	0.250	0.002	0.004	0.002
Contempt	-	-	-	-	0.946	0.835	0.887	0.835	-	-	-	-

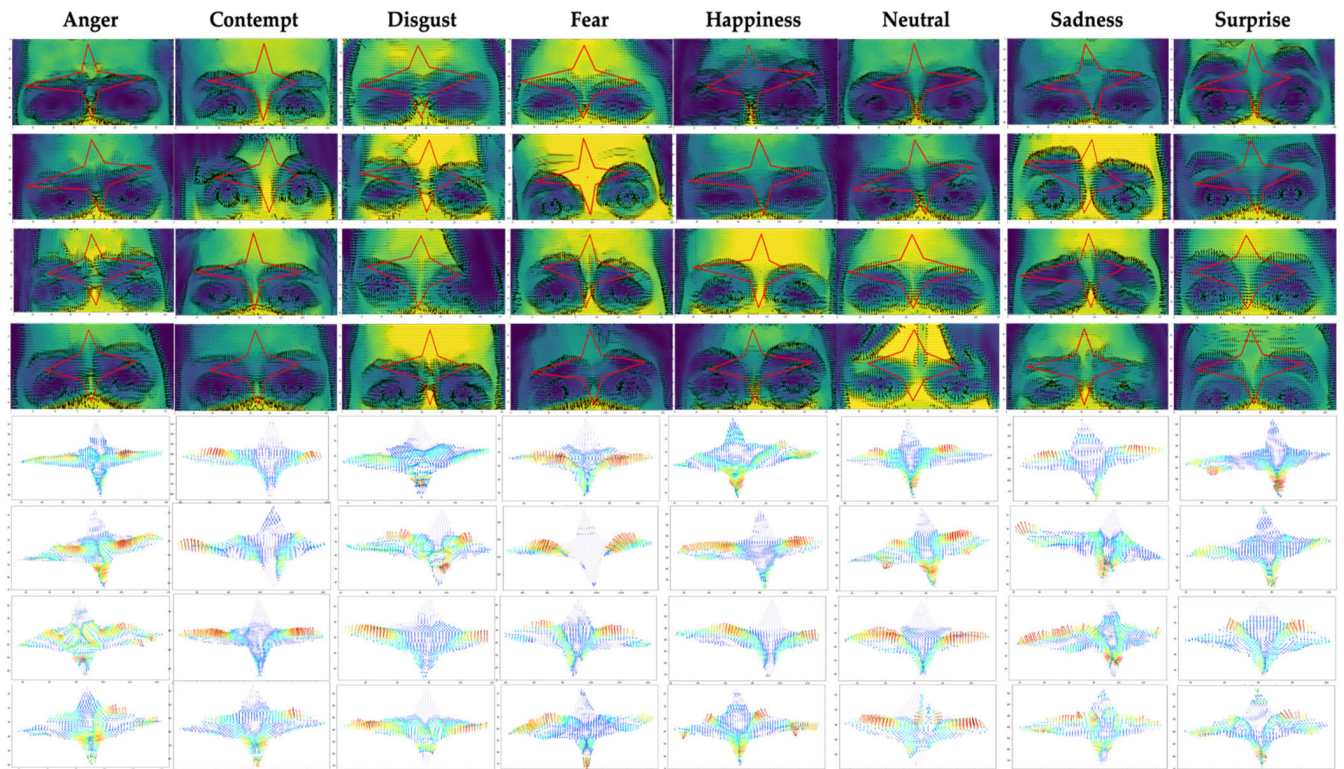


FIGURE 18. Samples of Star-Like Particle Polygon.

hand, while the other labels each have nearly 5,000 sample images, the Disgust expression only has 600 images.

The Real-World Affective Faces Database (RAF-DB), on the other hand, is one of the most extensive face expression databases available. Approximately 30,000 facial images are available in RAF-DB. The images were obtained from online resources. There are 40 annotators separately added

simple or compound statements to each image. Age, gender, ethnicity, head posture, illumination, occlusion (such as glasses, facial hair, or self-occlusion), and post-processing techniques all differ greatly among the images. The data set comprised five age brackets: 0–3, 4–19, 20–39, 40–69, and 70+. Furthermore, the proposed method’s accuracy metrics for FER2013, CK+ and RAF-DB are presented in Table 4.

However, Contempt does not exist in FER2013 and RAF-DB dataset.

By using our proposed SLPPE, each emotion has the variety of patterns including directions and magnitudes. Because of the flexibility of translation, rotation, and scaling invariance, each detected SLPPE has different shape and size. From the experiment, Neutral and Happiness's detected star-like polygon's ends are symmetric, but Neutral has less rotation than Happiness. For Anger, Disgust, Fear, and Sadness, the bridge of the nose happens to be greater multiple activated vectors compared to other emotions. Last but not least, Surprise's detected features do not have much of the eyebrow area, due to the fact that they are raised up significantly high from the eyes compared to the others. More importantly, in Fig. 18, the samples of our proposed Star-Like Particle Polygon in each emotion are depicted. It shows the activated area of all samples of CK+ dataset. Each area of the polygon of each emotion varies by the emotion.

More importantly, in order to demonstrate the performance achieved by the proposed SLPPE features and our end-to-end model architecture, the ablation studies were performed. As shown in Fig. 12 – Fig. 17, each module was excluded and the performing result was presented. Once each module was excluded, the performance on FER2013 and RAF-DB dataset were not the ideal results. The loss and validate loss were significantly decreasing when they started to increase to the wrong direction at approximately epoch 20th. On the other hand, the accuracy and validate accuracy were significantly increasing to approximately epoch 20th and ended up decreasing to the same level as the starting epoch. Additionally, the directions of the loss and accuracy learning curves on CK+ dataset were moving slowly to the ideal level and the learning performance were unstable.

According to the performances shown in Fig. 12 – Fig. 17 and the results presented in Table 4 – Table 10, our proposed end-to-end model architecture shown in Fig. 9 is the ideal structure for our proposed SLPPE features that produce significant result among FER2013, CK+, and RAF-DB datasets with the minimum number of learning parameters. The proposed end-to-end model architecture is compact and not able to adopt any further pruning process. Discarding any module from the proposed modules will lead to significantly lower result on at least one of the three datasets. Thus, each and every module of our proposed end-to-end model architecture is essential.

IV. CONCLUSION

The effectiveness of current methods of facial expression identification is significantly impacted by the necessity of using a face mask during the Covid-19 outbreak. In this study, we propose an emotion recognition technique based on star-like particle polygon estimation for partial facial images that consists of three key components. Firstly, a synthetic mask is used to conceal to lower part of the facial input image. The regional representation approach is adopted with only the upper part of the image. Secondly, in order to

extract a probability-based vectors of features that efficiently manifest the occluded facial image's properties, our Star-Like Particle Polygon Estimation (SLPPE) based feature extraction technique is utilized. Unlike other CNN based methods that bring the input image known as a raster form into several Conv modules in order to perform feature extraction process, we extract features from the original input image using our proposed SLPPE feature extraction technique in order to eliminate the issues of extracting unexpected features caused by the facial mask region provided by the Conv modules. Our proposed SLPPE feature extraction module produce the potential transformed data in the form of feature vectors without applying Conv modules. Lastly, the SLPPE is applied to the dataset of FER2013, CK+, and RAF-DB in order to evaluate our proposed technique. By using LSTM and ANN, the retrieved features are subsequently utilized in the classification process. More importantly, the SLPPE vectors are extracted from the scope of our proposed Star-Like Polygon area that is significantly translation, rotation, and scaling invariance. So, only a number of essential vectors are extracted among all existing vectors of the upper face. As a result, our proposed method outperforms the common CNN approaches and provides greater results with accuracy of 98.7%, 99.01%, and 94.62% on FER2013, CK+, and RAF-DB, respectively.

REFERENCES

- [1] M. Sajjad, F. U. M. Ullah, M. Ullah, G. Christodoulou, F. A. Cheikh, M. Hijji, K. Muhammad, and J. J. P. C. Rodrigues, "A comprehensive survey on deep facial expression recognition: Challenges, applications, and future guidelines," *Alexandria Eng. J.*, vol. 68, pp. 817–840, Apr. 2023.
- [2] A. Y. A. Maghari, "Recognition of partially occluded faces using regularized ICA," *Inverse Problems Sci. Eng.*, vol. 29, no. 8, pp. 1158–1177, Aug. 2021.
- [3] S. Al-Darraj, K. Berns, and A. Rodić, "Action unit based facial expression recognition using deep learning," in *Proc. Adv. Robot Design Intell. Control, 25th Conf. Robotics Alpe-Adria-Danube Region (RAAD)*, 2017, pp. 413–420.
- [4] S. Ziccardi, F. Crescenzo, and M. Calabrese, "What is hidden behind the mask? Facial emotion recognition at the time of COVID-19 pandemic in cognitively normal multiple sclerosis patients," *Diagnostics*, vol. 12, no. 1, p. 47, Dec. 2021.
- [5] Y. Nan, J. Ju, Q. Hua, H. Zhang, and B. Wang, "A-MobileNet: An approach of facial expression recognition," *Alexandria Eng. J.*, vol. 61, no. 6, pp. 4435–4444, Jun. 2022.
- [6] J. Zhang and H. Yu, "Improving the facial expression recognition and its interpretability via generating expression pattern-map," *Pattern Recognit.*, vol. 129, Sep. 2022, Art. no. 108737.
- [7] C. Bisogni, A. Castiglione, S. Hossain, F. Narducci, and S. Umer, "Impact of deep learning approaches on facial expression recognition in healthcare industries," *IEEE Trans. Ind. Informat.*, vol. 18, no. 8, pp. 5619–5627, Aug. 2022.
- [8] Y. Liu, C. Feng, X. Yuan, L. Zhou, W. Wang, J. Qin, and Z. Luo, "Clip-aware expressive feature learning for video-based facial expression recognition," *Inf. Sci.*, vol. 598, pp. 182–195, Jun. 2022.
- [9] H. Ge, Z. Zhu, Y. Dai, B. Wang, and X. Wu, "Facial expression recognition based on deep learning," *Comput. Methods Programs Biomed.*, vol. 215, Mar. 2022, Art. no. 106621.
- [10] J. Y. Ramirez Cornejo and H. Pedrini, "Emotion recognition from occluded facial expressions using Weber local descriptor," in *Proc. 25th Int. Conf. Syst., Signals Image Process. (IWSSIP)*, Jun. 2018, pp. 1–5.
- [11] L. Yan, Y. Shi, M. Wei, and Y. Wu, "Multi-feature fusing local directional ternary pattern for facial expressions signal recognition based on video communication system," *Alexandria Eng. J.*, vol. 63, pp. 307–320, Jan. 2023.

- [12] Z. Li, T. Zhang, X. Jing, and Y. Wang, "Facial expression-based analysis on emotion correlations, hotspots, and potential occurrence of urban crimes," *Alexandria Eng. J.*, vol. 60, no. 1, pp. 1411–1420, Feb. 2021.
- [13] A. Shukla, S. Petridis, and M. Pantic, "Does visual self-supervision improve learning of speech representations for emotion recognition?" *IEEE Trans. Affect. Comput.*, vol. 14, no. 1, pp. 406–420, Jan. 2023.
- [14] P. Lucey, J. F. Cohn, T. Kanade, J. Saragih, Z. Ambadar, and I. Matthews, "The extended Cohn-Kanade dataset (CK+): A complete dataset for action unit and emotion-specified expression," in *Proc. IEEE Comput. Soc. Conf. Comput. Vis. Pattern Recognit. Workshops*, Jun. 2010, pp. 94–101.
- [15] D. E. King, "Dlib-ML: A machine learning toolkit," *J. Mach. Learn. Res.*, vol. 10, pp. 1755–1758, Jul. 2009.
- [16] I. J. Goodfellow, D. Erhan, P. L. Carrier, A. Courville, M. Mirza, B. Hamner, and Y. Bengio, "Challenges in representation learning: A report on three machine learning contests," in *Proc. Neural Inf. Process., 20th Int. Conf. (ICONIP)*. Cham, Switzerland: Springer, 2013, pp. 117–124.
- [17] S. Li, W. Deng, and J. Du, "Reliable crowdsourcing and deep locality-preserving learning for expression recognition in the wild," in *Proc. IEEE Conf. Comput. Vis. Pattern Recognit. (CVPR)*, Jul. 2017, pp. 2584–2593.
- [18] V. Tümen, Ö. F. Söylemez, and B. Ergen, "Facial emotion recognition on a dataset using convolutional neural network," in *Proc. Int. Artif. Intell. Data Process. Symp. (IDAP)*, Sep. 2017, pp. 1–5.
- [19] A. T. Kabakus, "PyFER: A facial expression recognizer based on convolutional neural networks," *IEEE Access*, vol. 8, pp. 142243–142249, 2020.
- [20] A. G. Howard, M. Zhu, B. Chen, D. Kalenichenko, W. Wang, T. Wey, M. Andreetto, and H. Adam, *Mobilenets*.
- [21] C. Szegedy, W. Liu, Y. Jia, P. Sermanet, S. Reed, D. Anguelov, D. Erhan, V. Vanhoucke, and A. Rabinovich, "Going deeper with convolutions," in *Proc. IEEE Conf. Comput. Vis. Pattern Recognit. (CVPR)*, Jun. 2015, pp. 1–9.
- [22] K. He, X. Zhang, S. Ren, and J. Sun, "Deep residual learning for image recognition," in *Proc. IEEE Conf. Comput. Vis. Pattern Recognit. (CVPR)*, Jun. 2016, pp. 770–778.
- [23] F. Chollet, "Xception: Deep learning with depthwise separable convolutions," in *Proc. IEEE Conf. Comput. Vis. Pattern Recognit. (CVPR)*, Jul. 2017, pp. 1800–1807.
- [24] J. Shao and Y. Qian, "Three convolutional neural network models for facial expression recognition in the wild," *Neurocomputing*, vol. 355, pp. 82–92, Aug. 2019.
- [25] M. N. Riaz, Y. Shen, M. Sohail, and M. Guo, "EXnet: An efficient approach for emotion recognition in the wild," *Sensors*, vol. 20, no. 4, p. 1087, Feb. 2020.
- [26] Y. Li, J. Zeng, S. Shan, and X. Chen, "Patch-gated CNN for occlusion-aware facial expression recognition," in *Proc. 24th Int. Conf. Pattern Recognit. (ICPR)*, Aug. 2018, pp. 2209–2214.
- [27] Y. Li, J. Zeng, S. Shan, and X. Chen, "Occlusion aware facial expression recognition using CNN with attention mechanism," *IEEE Trans. Image Process.*, vol. 28, no. 5, pp. 2439–2450, May 2019.
- [28] Y. Gan, J. Chen, Z. Yang, and L. Xu, "Multiple attention network for facial expression recognition," *IEEE Access*, vol. 8, pp. 7383–7393, 2020.
- [29] H. Yang, U. Ciftci, and L. Yin, "Facial expression recognition by de-expression residue learning," in *Proc. IEEE/CVF Conf. Comput. Vis. Pattern Recognit.*, Jun. 2018, pp. 2168–2177.
- [30] S. Jyoti, G. Sharma, and A. Dhall, "Expression empowered ResiDen network for facial action unit detection," in *Proc. 14th IEEE Int. Conf. Autom. Face Gesture Recognit. (FG)*, May 2019, pp. 1–8.
- [31] S. Miao, H. Xu, Z. Han, and Y. Zhu, "Recognizing facial expressions using a shallow convolutional neural network," *IEEE Access*, vol. 7, pp. 78000–78011, 2019.
- [32] G. Zhao, H. Yang, and M. Yu, "Expression recognition method based on a lightweight convolutional neural network," *IEEE Access*, vol. 8, pp. 38528–38537, 2020.
- [33] B. Pan, S. Wang, and B. Xia, "Occluded facial expression recognition enhanced through privileged information," in *Proc. 27th ACM Int. Conf. Multimedia*, Oct. 2019, pp. 566–573.
- [34] K. Wang, X. Peng, J. Yang, D. Meng, and Y. Qiao, "Region attention networks for pose and occlusion robust facial expression recognition," *IEEE Trans. Image Process.*, vol. 29, pp. 4057–4069, 2020.
- [35] K. Wang, X. Peng, J. Yang, S. Lu, and Y. Qiao, "Suppressing uncertainties for large-scale facial expression recognition," in *Proc. IEEE/CVF Conf. Comput. Vis. Pattern Recognit. (CVPR)*, Jun. 2020, pp. 6896–6905.
- [36] H. Ding, P. Zhou, and R. Chellappa, "Occlusion-adaptive deep network for robust facial expression recognition," in *Proc. IEEE Int. Joint Conf. Biometrics (IJCB)*, Sep. 2020, pp. 1–9.
- [37] A. H. Farzaneh and X. Qi, "Facial expression recognition in the wild via deep attentive center loss," in *Proc. IEEE Winter Conf. Appl. Comput. Vis. (WACV)*, Jan. 2021, pp. 2401–2410.



RATANAK KHOEUN received the B.Sc. degree in computer science and the M.Sc. degree in informatics from Burapha University, Chonburi, Thailand, in 2015 and 2017, respectively, where he is currently pursuing the Ph.D. degree in informatics. His research interests include image processing and digital geometry processing.



WATCHARAPHONG YOOKWAN received the B.Sc. degree in computer science, the M.Sc. degree in informatics from Burapha University, Chonburi, Thailand, in 2016 and 2018, respectively, and the Ph.D. degree in computer engineering from the Suranaree University of Technology University, Thailand, in 2022. His research interests include image processing and digital geometry processing.



PONLAWAT CHOPHUK received the B.Eng. degree in electronic engineering, the M.Eng. degree in biomedical engineering from the King Mongkut's Institute of Technology Ladkrabang, in 2014 and 2016, respectively, and the Ph.D. degree in electrical and information engineering technology from the King Mongkut's University of Technology Thonburi, Thailand, in 2022. His current research interests include computer vision, image processing, human computer interaction, and machine learning.



ANNUPAN RODTOOK received the M.Sc. degree in computer science from the Mongkut's Institute of Technology Ladkrabang, Thailand, in 1996, and the Ph.D. degree in technology from the Sirindhorn International Institute of Technology, Thammasat University, Thailand, in 2005. He is currently an Associate Professor with the Computer Science Department, Ramkhamhaeng University, Thailand. His research interests include image processing, medical image processing, and pattern recognition.



KRISANA CHINNASARN (Senior Member, IEEE) received the B.Sc. degree in statistics from Srinakharinwirot University, Mahasarakham Campus, Thailand, in 1992, the M.Sc. degree in computer science and information technology from the King Mongkut's Institute of Technology Ladkrabang, Thailand, in 1997, and the Ph.D. degree in computer science from Chulalongkorn University, Thailand, in 2004. From 1996 to 1997, he was a Research Assistant with the Computer Center, King Mongkut Institute of Technology Ladkrabang. From 2002 to 2003, he visited the Oxford University Computing Laboratory, Oxford, U.K., as a Ph.D. Visiting Student. Since 1997, he has been a Lecturer with the Faculty of Informatics, Burapha University, where he is currently a former of the Department of Computer Science, Faculty of Science. He has been an Assistant Professor of computer science, since 2006. His research interests include machine learning and digital image processing and their applications to other science and engineering areas.